

3D multi-objective optimization of hybrid composite laminates: Influence of fiber orientation and stacking sequence

Ibrahim Beroual^a, Moussa Amadji^{b,c*} and Djamel Haddad^b

^aLaboratory of Mechanics, Structures and Energetics (LMSE), Faculty of Construction Engineering, Mouloud Mammeri University, BP 17 RP Tizi-Ouzou, Algeria

^bInstitute of Industrial Hygiene and Safety, University Chadid Mostefa Ben Boulaïd Batna 2, Batna 05000, Algeria

^cLaboratory of Mechanics of Structures & Materials (LMSM), University Chadid Mostefa Ben Boulaïd Batna 2, Batna 05000, Algeria

ARTICLE INFO

Article history:

Received 10 January 2026

Accepted 22 February 2026

Available online

22 February 2026

Keywords:

Genetic algorithm

Hybrid composites

Optimization

Finite element method (FEM)

ANSYS

ABSTRACT

Hybrid laminated composites, integrating High Strength (HS) carbon and glass fibers (E, S) within an epoxy matrix, deliver an optimal compromise between lightweight design, mechanical strength, and cost-effectiveness for applications in industrial, aerospace, automotive, and civil engineering sectors. This study presents a three-dimensional optimization of mechanical performance through a multi-objective genetic algorithm (MOGA) under static loading conditions. The design variables encompass the number of plies (6 to 12), fiber orientation angles ($-90^\circ \leq \theta \leq 90^\circ$), and ply materials: HS-Carbon/Epoxy (CF-EP), E-Glass/Epoxy (EG-EP) and S-Glass/Epoxy (SG-EP). A constraint mandating 25% CF-EP placement at the core to maximize stiffness while minimizing stresses. The objectives are to enhance the longitudinal modulus (E_x) and reduce von-Mises stress, while ensuring compliance with the Tsai-Wu failure criterion. An analytical model, implemented in MATLAB, incorporates stiffness matrices, Tsai-Wu failure indices, and von-Mises stress calculations, demonstrating a 30% increase in stiffness and effective mitigation of stress concentrations through centralized CF-EP placement. These findings are corroborated by finite element method (FEM) simulations conducted in ANSYS, which exhibit strong agreement with analytical predictions. This hybrid methodology offers a strong framework for developing high-performance laminated composites, significantly impacting applications requiring structural reliability and efficiency.

© 2026 Growing Science Ltd. All rights reserved.

1. Introduction

Composite materials are revolutionizing high-tech industries due to their exceptional mechanical performance and lightweight properties, yet their optimization remains a significant challenge (Anto et al., 2019). A composite material is formed by combining at least two chemically distinct substances, referred to as constituent materials, which are categorized into two distinct phases: the matrix, a continuous and typically more flexible phase, and the reinforcement, a discontinuous phase characterized by its hardness and enhanced strength (Anto et al., 2019). The primary advantage of composites lies in their ability to tailor properties: the matrix, serving as the primary support, incorporates fibers or particles to meet specific requirements, such as tensile strength, wear resistance, optimized density, high-temperature performance, surface hardness, dimensional stability, or effective vibration damping (Sabau et al., 2017). Among reinforcements, high-modulus (HM) carbon fibers exhibit a Young's modulus exceeding 300 GPa, while high-strength (HS) fibers, being more cost-effective, are commonly used in industrial or recreational applications, particularly for non-structural aircraft components. Compared to glass fiber composites, these reinforcements deliver superior mechanical performance, with weight reductions of up to 40% (Vlase et al., 2011). Kevlar 49 aramid fiber, known for its low density and high mechanical strength, plays a critical role in plastic composites, particularly in fields such as aeronautics, aerospace, marine, automotive, and sports equipment. Available as continuous yarns, chopped fibers, or fabrics, it ensures lightweight structures with excellent stiffness. Hybrid composites, developed by combining various reinforcements within a single matrix, enable the creation of structures with finely tuned properties, mitigating the individual limitations of materials. The incorporation of natural fibers makes them more cost-

* Corresponding author.

E-mail addresses: m.amadji@univ-batna2.dz (M. Amadji)

effective and environmentally friendly, with their performance evaluated using the rule of mixtures and the Tsai-Wu failure criterion, positioning them as highly valued and rapidly developing solutions (Shaikh et al., 2022). Polymer matrix composites, such as carbon/epoxy or glass/epoxy, stand out in aerospace and other mechanical sectors due to their high stiffness, exceptional strength, and corrosion resistance, surpassing metals. While carbon fiber excels in durability, its cost drives hybridization with glass/epoxy, and their lightweight nature enhances efficiency across numerous applications (Satkar et al., 2022; Mache et al., 2013). Technical calculations are fundamental to design, whether related to structural or technological aspects. The diverse challenges faced by engineers have led to the development of multiple calculation methods, refined over decades through theoretical and technological advancements (Gdoutos, Emmanuel E, 2005). The finite element method (FEM) has emerged as the primary numerical approach in engineering. Finite element analysis (FEA) models physical systems using partial differential equations (Hutton, David V, 2004). To achieve this, the analyzed domain is discretized into a mesh of finite elements, transforming the real system into a discrete structure suitable for numerical analysis. Specialized software, such as ANSYS, leverages the power of FEM to streamline this discretization process and integrates seamlessly with computer-aided design environments, delivering accurate solutions for complex simulations (Barbero et Cortes, 2010). These advanced numerical tools play a pivotal role in the optimization of composites, a field where mechanical performance depends on numerous complex parameters.

The optimization of laminated composite materials is a critical research area in engineering, particularly due to their widespread use in demanding applications such as aerospace and mechanical engineering (Monte et al., 2017). Unlike homogeneous materials, laminated composite structures exhibit increased complexity stemming from the diversity of design parameters, including ply thickness, fiber orientation, and volume fraction. These factors directly influence mechanical performance, notably stiffness, buckling resistance, and mass (Henrichsen, Søren Randrup, 2015). The optimization process for composites is particularly challenging due to the large number of variables involved and their nonlinear interactions (Monte et al., 2017). Typically, in optimization problems for composite laminates, fiber orientation angles and ply thickness are considered key design variables (Lin, et Lee 2004; Riccio et al. 2024). These parameters are optimized to reduce structural weight (Yibre et al. 2020) and manufacturing costs (Riccio et al., 2024; Kaufmann et Mattei, 2008). Other researchers (Aymerich et al., 2008; Chang et al., 2010) have focused on optimizing the stacking sequence (OSS) of laminates to significantly enhance their mechanical properties without affecting weight. Furthermore, the analytical and numerical models used to evaluate the behavior of composite structures require computationally intensive calculations. To minimize the need for experimental trials, several mathematical optimization methods have been developed, including the genetic algorithm (GA), ant colony optimization (ACO) (Aymerich et al., 2008), and particle swarm optimization (PSO) (Chang et al., 2010; Suresh et al., 2007; Huang et al., 2017).

Hybrid laminates, combining high-performance fibers with organic matrices, are transforming structural engineering due to their exceptional stiffness and lightweight properties. Current research leverages multi-objective genetic algorithms (MOGA) and advanced finite element method (FEM) simulations to optimize fiber arrangements and orientations, enabling effective resistance to static and/or dynamic loads. Bertan Beylergil (2020) investigated the optimization of hybrid composite laminates using MOGA and ANSYS, integrating bending-torsion objectives while considering natural frequencies, the Tsai-Wu failure index, cost, and weight. The results demonstrate that an increased proportion of E-glass fibers reduces costs while enhancing mechanical performance, with numerical simulations minimizing the need for costly experimental trials, thus offering an effective balance between stiffness and cost. Prashant S. Hatti et al. (2022) evaluated the performance of hybrid composite laminates through finite element analysis (FEA), analytical calculations, and experimental testing, revealing that load-bearing capacity increases with fiber orientations at 45° and 90°, although tensile stress decreases with the number of layers. Madhu Kumar K.P. et al. (2020) analyzed hybrid composite laminates (E/S-glass, 70%/30% polyester matrix) by fabricating standard specimens and conducting experimental tests on conductivity, dielectric tensile strength, and abrasion, demonstrating improved mechanical properties. Zheng Zhang et al. (2021) employed the NSGA-II algorithm for multi-objective optimization of bistable laminates, developing controllable configurations that enhance structural adaptability under variable loads, though their study focused on general performance. Ramesh Kumpati et al. (2024) advanced this field by using multi-objective genetic algorithms to optimize composite laminates, achieving improved stacking sequences for resisting failure loads, but without incorporating specific fiber placement constraints required for high-stiffness applications. Michał Stosiak et al. (2025) explored the design of a composite hydraulic cylinder using genetic algorithms, achieving a 15% increase in stiffness through optimized fiber positioning, although their research did not account for specific placement constraints necessary for hybrid laminates with high-stiffness fibers. Bhaskar Reddy et al. (2023) conducted a study to evaluate the mechanical properties of S-glass and E-glass composites with an epoxy resin matrix, considering three fiber orientations: [0°/90°], [+45°/-45°], and [0°/45°/90°]. The objective was to analyze the impact of fiber orientation on tensile and flexural strength through experimental testing and finite element method (FEM) simulations using ABAQUS. The goal was to optimize these composites for aerospace and automotive applications. M. Meng et al. (2015) investigated the effect of fiber arrangement on the flexural failure of CFRP laminates ([0]₁₆, [0/90]_{4s}, [±45]_{4s}) using 3D finite element analysis (FEA) based on the Tsai-Hill criterion, an extended classical lamination theory (CLT), and ISO three-point bending tests to analyze failure initiation. They identified transverse (cross-ply) and shear (angle-ply) stresses near free edges, explaining the loss of stiffness observed under microscopy. The 3D FEA outperformed 2D models, demonstrating that all six stress components influence failure modes: micro-buckling (unidirectional), enhanced by a transverse layer (cross-ply), and torsion (angle-ply). Fiber angles of 10-13° maximize stresses and should be avoided on the surface. Edge effects, more pronounced in angle-ply

laminates and short spans, converge toward CLT predictions at the center. They recommend transverse layers to enhance flexural performance.

This study presents a multi-objective optimization framework for carbon/glass-epoxy hybrid laminates, implemented using a multi-objective genetic algorithm (MOGA) in MATLAB. The framework optimizes key variables, including fiber orientation ($-90^\circ \leq \theta \leq 90^\circ$), number of layers (6 to 12), and material stacking sequence (E-glass, S-glass, HS-carbon), with a constraint mandating 25% carbon plies positioned at the core to maximize stiffness and reduce stress concentrations. By targeting the maximization of the effective longitudinal modulus (E_x), minimization of the von-Mises stress, and compliance with the Tsai-Wu failure criterion, the framework integrates 3D numerical analyses and stiffness matrix formulations. Finite element simulations conducted in ANSYS demonstrate that optimal solutions can increase stiffness by up to 30% and significantly reduce stresses, providing a scalable methodology for aerospace, automotive, and structural applications.

2. Theoretical

2.1 Mathematical formulas

The link between Hooke's law, which describes the elastic stress-strain relationship, and the linear proportional behavior of stress and strain in elastic materials, is demonstrated mathematically in the research works (Berthelot, 2005; Daniel et al., 1994).

$$\sigma_{ij} = C_{ijkl}\epsilon_{kl} \quad (1)$$

where C_{ijkl} is a fourth-order tensor with 81 elastic constants, and the inverted form of Hooke's law in the case of orthotropic material, as detailed in reference (Merhar, 2020).

$$\epsilon_i = S_{ij}\sigma_j \quad (2)$$

Coefficients S_{ij} are called compliance coefficients which is the inverse of the stiffness matrix (Merhar, M., 2020).

$$S_{ij} = C_{ij}^{-1} \quad (3)$$

The constitutive Eq. (2) of an orthotropic material can be translated into matrix form (Merhar, M., 2020).

$$\begin{bmatrix} \epsilon_1 \\ \epsilon_2 \\ \epsilon_3 \\ \gamma_{23} \\ \gamma_{13} \\ \gamma_{12} \end{bmatrix} = \begin{bmatrix} S_{11} & S_{12} & S_{13} & 0 & 0 & 0 \\ S_{21} & S_{22} & S_{23} & 0 & 0 & 0 \\ S_{31} & S_{32} & S_{33} & 0 & 0 & 0 \\ 0 & 0 & 0 & S_{44} & 0 & 0 \\ 0 & 0 & 0 & 0 & S_{55} & 0 \\ 0 & 0 & 0 & 0 & 0 & S_{66} \end{bmatrix} \begin{bmatrix} \sigma_1 \\ \sigma_2 \\ \sigma_3 \\ \tau_{23} \\ \tau_{13} \\ \tau_{12} \end{bmatrix} \quad (4)$$

where the engineering constants' individual compliance coefficients are (Merhar, M., 2020).

$$\begin{aligned} S_{11} &= 1/E_1, & S_{12} &= -\nu_{12}/E_2, & S_{13} &= -\nu_{31}/E_3, & S_{21} &= -\nu_{12}/E_1, & S_{22} &= 1/E_2, & S_{23} &= -\nu_{32}/E_3, \\ S_{31} &= -\nu_{13}/E_1, & S_{32} &= -\nu_{23}/E_2, & S_{33} &= 1/E_3, & S_{44} &= 1/G_{23}, & S_{55} &= 1/G_{13}, & S_{66} &= 1/G_{12}, \\ S_{ij} &= S_{ji} \end{aligned} \quad (5)$$

E_1, E_2, E_3 are the modulus of elasticity in the principal material (1-2-3) coordinate system (**Fig. 1**), G_{12}, G_{13}, G_{23} , shear modulus in and ν_{ij} Poisson's ratios (Merhar, M., 2020).

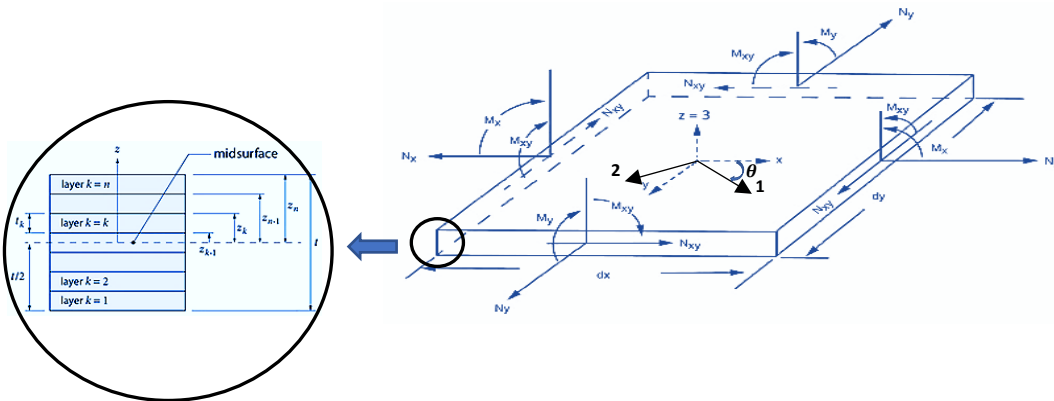


Fig. 1. The coordinate notation for individual plies in the multidirectional laminate, under forces and moments per unit length (Merhar, 2020).

When the principal material coordinate system does not coincide with the global x-y-z coordinate system, but it is rotated through an angle θ about the common z-(3) axis, as indicated in **Fig. 1**, the transformed compliance matrix can be defined as (Merhar, M., 2020).

$$[\bar{S}] = [T_2]^{-1} [S] [T_1] \quad (6)$$

$$[\bar{S}] = \begin{bmatrix} \bar{S}_{11} & \bar{S}_{12} & \bar{S}_{13} & 0 & 0 & \bar{S}_{16} \\ \bar{S}_{21} & \bar{S}_{22} & \bar{S}_{23} & 0 & 0 & \bar{S}_{26} \\ \bar{S}_{31} & \bar{S}_{32} & \bar{S}_{33} & 0 & 0 & \bar{S}_{36} \\ 0 & 0 & 0 & \bar{S}_{44} & \bar{S}_{45} & 0 \\ 0 & 0 & 0 & \bar{S}_{54} & \bar{S}_{55} & 0 \\ \bar{S}_{61} & \bar{S}_{62} & \bar{S}_{63} & 0 & 0 & \bar{S}_{66} \end{bmatrix} \quad (7)$$

Where the transformation matrices $[T_1]$ and $[T_2]$ are

$$T_1 = \begin{bmatrix} c^2 & s^2 & 0 & 0 & 0 & 2cs \\ s^2 & c^2 & 0 & 0 & 0 & -2cs \\ 0 & 0 & 1 & 0 & 0 & 0 \\ 0 & 0 & 0 & c & -s & 0 \\ 0 & 0 & 0 & s & c & 0 \\ -cs & cs & 0 & 0 & 0 & c^2 - s^2 \end{bmatrix} \quad (8)$$

$$T_2 = \begin{bmatrix} c^2 & s^2 & 0 & 0 & 0 & cs \\ s^2 & c^2 & 0 & 0 & 0 & -cs \\ 0 & 0 & 1 & 0 & 0 & 0 \\ 0 & 0 & 0 & c & -s & 0 \\ 0 & 0 & 0 & s & c & 0 \\ -2cs & 2cs & 0 & 0 & 0 & c^2 - s^2 \end{bmatrix} \quad (9)$$

where S is the compliance matrix of lamina; $c = \cos(\theta)$ and $s = \sin(\theta)$. Substituting the three-dimensional version of composites compliance matrix into CLT equations (Kaw, 2005). The fundamental equation, or load-deformation relation, of laminate analysis (Classical laminated theory, CLT) is presented in Eq. (10) as follows (Casavola et al., 2016):

$$\begin{Bmatrix} N \\ M \end{Bmatrix} = \begin{bmatrix} A & B \\ B & D \end{bmatrix} \begin{Bmatrix} \varepsilon^0 \\ k \end{Bmatrix}, \quad (10)$$

where $\{N\}$, $\{M\}$, $\{\varepsilon^0\}$, and $\{k\}$ represent the vectors of resultant forces, moments, midplane strains, and curvatures, respectively. The matrices $[A]$, $[B]$, and $[D]$ correspond to the extensional stiffness, coupling stiffness, and bending stiffness, respectively. For symmetrical laminates, the coupling matrix $[B]$, which connects extension and bending, is zero. The load-deformation relation in Classical Lamination Theory (CLT), is presented in Eq. (10) as follows, according to reference (Bertan Beylergil, 2020; M. Meng et al., 2015). The version of matrices $[A]$, $[B]$ and $[D]$ can be written as,

$$A_{ij} = \sum_{k=1}^n [\bar{Q}]_k (h_k - h_{k-1}) \quad (11.a)$$

$$B_{ij} = \frac{1}{2} \sum_{k=1}^n [\bar{Q}]_k (h_k^2 - h_{k-1}^2) \quad (11.b)$$

$$D_{ij} = \frac{1}{3} \sum_{k=1}^n [\bar{Q}]_k (h_k^3 - h_{k-1}^3) \quad (11.c)$$

$$h = \sum_{n=1}^k t_k \quad (11.d)$$

$$[\bar{Q}] = [\bar{S}]^{-1} \quad (12)$$

where n , t_k and $[\bar{Q}]_k$ are the total number of layers, the thickness of each layer and the transformed reduced stiffness matrix; respectively (M. Meng et al., 2015). The plane stresses constitutive equation allows for the calculation of stresses at any z -position within the k^{th} layer (Merhar, M., 2020):

$$\{\sigma\}_x = [\bar{Q}]_k \{\varepsilon\}_x \quad (13)$$

Converting the stresses from principal coordinates (x and y) to local coordinates is a necessary step in calculating von-Mises stresses and the Tsai-Wu failure criterion (Hwang et al., 2023):

$$\{\sigma\}_{12} = [T_2] \{\sigma\}_x \quad (14)$$

The conversion of strains from principal coordinates (x and y) to local coordinates is explained in Eq. (15),

$$\{\varepsilon\}_{12} = [T_1] \{\varepsilon\}_x \quad (15)$$

2.1.1 Longitudinal Young's modulus (E_x)

To calculate the effective Young's modulus (E_x) of a laminate, so we must solve the laminate Eq. (10) by reversing it (Casavola et al., 2016).

$$\begin{Bmatrix} \varepsilon^0 \\ k \end{Bmatrix} = \begin{bmatrix} A & B \\ B & D \end{bmatrix}^{-1} \begin{Bmatrix} N \\ M \end{Bmatrix} \quad (16)$$

Since this inversion can be complex, a simpler way is to invert the three tensors A , B and D from Eq. (16) one by one. This allows us to rewrite Eq. (16) as follows (Casavola et al., 2016):

$$\begin{Bmatrix} \varepsilon^0 \\ k \end{Bmatrix} = \begin{bmatrix} a & b \\ b^T & d \end{bmatrix}^{-1} \begin{Bmatrix} N \\ M \end{Bmatrix} \quad (17)$$

With;

$$\begin{aligned} a &= (A - BD^{-1}B)^{-1} \\ d &= (D - BA^{-1}B)^{-1} \\ b &= -aBD^{-1} = -(A - BD^{-1}B)^{-1}BD^{-1} \end{aligned} \quad (18)$$

To determine the laminate's properties, the following can be defined (Casavola et al., 2016):

$$a^* = ha \quad (19)$$

Thus, the laminate effective Young's Modulus in the x direction is (Casavola et al., 2016):

$$E_x = 1/a_{11}^* \quad (20)$$

In this study, using a genetic algorithm to optimize laminates based on CLT, the effective Young's modulus obtained for each optimized configuration can be compared to that calculated by the finite element method.

2.1.2 Stress von-Mises

The von-Mises stress is a critical criterion for analyzing plastic failure in long-fiber laminates, such as those made from carbon or glass fibers and epoxy resin, due to their anisotropic behavior under complex loading conditions. It facilitates the assessment of a global equivalent stress based on principal stresses, thereby providing a reliable indicator of the risk of permanent deformation or rupture in these heterogeneous composite materials (Jones, 1999). The optimization of this stress, often conducted using numerical methods such as multi-objective optimization algorithms, seeks to minimize the stress while enhancing essential mechanical properties, such as Young's modulus, to improve the stiffness and longevity of the laminates. This strategy is indispensable in demanding sectors like aerospace and automotive industries, where mechanical performance and safety are top priorities. The von-Mises stress is determined by the following formula (Wang et al., 2019):

$$\sigma_{\text{VonMises}} = \sqrt{\frac{1}{2} \left((\sigma_x - \sigma_y)^2 + (\sigma_y - \sigma_z)^2 + (\sigma_z - \sigma_x)^2 \right) + 3(\tau_{xy}^2 + \tau_{yz}^2 + \tau_{xz}^2)} \quad (21)$$

where $(\sigma_x, \sigma_y$ and $\sigma_z)$ shows the normal stresses and $(\tau_{xy}, \tau_{yz}$ and $\tau_{xz})$ are the shear stresses in the respective directions.

2.1.3 Tsai-Wu failure criterion

To evaluate the progressive degradation of each layer in a hybrid composite laminate, the Tsai-Wu failure criterion was used in this study. This criterion, one of the most commonly used for anisotropic materials like laminated composites, is widely adopted by researchers and designers for many composite structures for decades. It has been successfully integrated into finite element software such as Abaqus and ANSYS. The failure index (FI) for each composite layer is calculated using Eq. (22) (Beylegil, 2011). The material is considered safe if $FI \leq 1$, but layer failure occurs if $FI \geq 1$.

$$FI = F_1\sigma_1 + F_2\sigma_{21} + F_3\sigma_3 + F_{11}\sigma_1^2 + F_{22}\sigma_2^2 + F_{33}\sigma_3^2 + F_{44}\sigma_4^2 + F_{55}\sigma_5^2 + F_{66}\sigma_6^2 + 2F_{12}\sigma_1\sigma_2 + 2F_{13}\sigma_1\sigma_3 + 2F_{23}\sigma_2\sigma_3 \quad (22)$$

$$\begin{aligned} F_1 &= 1/X_t + 1/X_c; & F_2 &= 1/Y_t + 1/Y_c \\ F_3 &= 1/Z_t + 1/Z_c; & F_{11} &= -1/X_t \times X_c \\ F_{22} &= -1/Y_t \times Y_c; & F_{33} &= -1/Z_t \times Z_c \\ F_{44} &= 1/S_{23}^2; & F_{55} &= 1/S_{13}^2 \\ F_{66} &= 1/S_{12}^2; & F_{12} &= -\frac{1}{2}\sqrt{F_{11} \times F_{22}}; \\ F_{23} &= -\frac{1}{2}\sqrt{F_{22} \times F_{33}}; & F_{13} &= -\frac{1}{2}\sqrt{F_{11} \times F_{33}} \end{aligned} \quad (23)$$

In Eq. (23), X , Y , and Z represent the material strengths in the x , y , and z directions, respectively, where the subscripts t and c denote tensile and compressive strengths, respectively. S denotes the shear strength of the composite laminate. The tensile, compressive, and shear strength values for the SG-EP, EG-EP, and CF-EP composites are widely available in the literature, as indicated in references (Zhang et al., 2011; Zhao et Xue, 2014; Shokrieh, et Lessard, 2000). For this study, we use the values available in the ANSYS Workbench 16.2 library as shown in Table 1, as the characteristics of the materials used also originate from this library, where negative values indicate compressive strength.

Table 1. Material properties of reinforced epoxy laminates.

Properties (ANSYS Inc, 2015)	E-Glass/epoxy	S-Glass/epoxy	HS-Carbon/epoxy
Young's Modulus in X-direction (MPa)	40000	50000	121000
Young's Modulus in Y-direction (MPa)	10000	8000	8600
Young's Modulus in Z-direction (MPa)	10000	8000	8600
Poisson's ratio in XY-plane	0.3	0.3	0.27
Poisson's ratio in YZ-plane	0.3	0.3	0.27
Poisson's ratio in XZ-plane	0.4	0.4	0.4
Shear Modulus in XY-plane (MPa)	5000	5000	4700
Shear Modulus in YZ-plane (MPa)	5000	5000	4700
Shear Modulus in XZ-plane (MPa)	3846	3846	3100
Orthotropic stress Limits			
Tensile strength in X-direction (MPa)	1100	1700	2231
Tensile strength in Y-direction (MPa)	35	35	29
Tensile strength in Z-direction (MPa)	35	35	29
Compressive strength in X-direction (MPa)	-675	-1000	-1082
Compressive strength in Y-direction (MPa)	-120	-120	-100
Compressive strength in Z-direction (MPa)	-120	-120	-100
Shear strength in XY-plane (MPa)	80	80	60
Shear strength in YZ-plane (MPa)	46.15	46.15	32
Shear strength in XZ-plane (Ma)	80	80	60

3. Problem statement

In this study, 3D numerical analyses of a hybrid composite plate, composed of layers of glass-E/epoxy (EG-EP), glass-S/epoxy (SG-EP), and HS-carbon/epoxy (CF-EP) composites, were performed using ANSYS Workbench with the ACP module. The objective was to optimize the laminate to maximize the Young's modulus and minimize the von-Mises stress, while respecting a Tsai-Wu failure criterion ≤ 0.7 . The optimization was carried out using a multi-objective genetic algorithm

implemented in MATLAB. The plate, with dimensions of 200 mm in length and 100 mm in width, was subjected separately to tensile (axial and biaxial) and compressive (axial and biaxial) loadings, applied uniformly without eccentricity. Axial loadings were applied on two opposite sides, while biaxial loadings involved all four sides. The finite element model was analytically validated using our existing MATLAB model to ensure mesh independence. The hybrid composite plate consisted of 6 to 12 layers, with a total thickness of 3 mm, each layer having a thickness adapted to meet this constraint. The fiber orientations varied between -90° to 90° . A design constraint required that 25% of the laminate be concentrated at the center of the laminate, be made of carbon/epoxy. The materials used were EG-EP, SG-EP, and CF-EP. The mechanical properties of the composites are detailed in Table 1. The results, including the von-Mises stress and the Young's modulus, are presented in the results and discussion section.

4. Multi-Objective genetic algorithm

4.1 Genetic algorithm

The Multi-Objective Genetic Algorithm (MOGA) is a computer method that solves problems with multiple different goals (Deb, 2001). Instead of finding one perfect solution, MOGA looks for a set of good solutions called the Pareto front. This front shows the trade-offs between goals and offers several possible options. MOGA uses ideas from genetics, like crossover, mutation, and selection, to improve a group of solutions over time. Each solution is judged based on multiple criteria, and the best ones are kept to create new solutions. MOGA is very helpful in engineering and design, such as for optimizing structures, managing resources, or modeling complex systems. This method helps decision-makers pick the best solution for their needs. A multi-criteria optimization problem can be described as follows (Bugada castelltort, 2012):

Maximize/minimize

$$f_i(x), i = 1, \dots, N \quad (24)$$

subject to constraints

$$g_j(x) = 0, \quad j = 1, \dots, M \quad (25)$$

$$h_k(x) \leq 0 \quad k = 1, \dots, W \quad (26)$$

where f_i , g_j , and h_k represent the objective functions, equality constraints, and inequality constraints, respectively. N denotes the number of objective functions, and x is an n -dimensional vector. The Genetic Algorithm (GA) is a computer method that mimics natural selection and genetics to find solutions. Genes and chromosomes are the main components. A chromosome is a sequence of genes. In a real problem, genes are the things to improve, and a chromosome is a possible solution. GAs search for the best solution by testing many chromosomes. They have advantages: they can test multiple solutions at once and temporarily accept fewer good solutions, which prevents getting stuck on an average solution (Anam, 2019). GAs are great for complex problems because they easily turn variables into genetic sequences to form chromosomes. They explore different paths by keeping a group of possible solutions. Through operations like crossover and mutation, they offer alternative solutions, even if the best one isn't perfect for reasons not considered. This makes GAs very useful for designing and optimizing composite structures, like those with layers of materials with complex properties (Bertan Beylergil, 2020; Albadr et al., 2020).

A Genetic Algorithm for multiple goals is called a Multi-Objective Genetic Algorithm (MOGA). MOGA is an improved version of an algorithm called NSGA-II, which uses elitism to pick the best solutions (Zheng Zhang et al., 2021). Here's how it works: it starts by creating a random group of solutions, then evaluates each one, selects the best, mixes them (crossover), and changes them (mutation). Elitism helps keep the best solutions to create new ones. If the results aren't good enough, it starts over. In the end, it provides a set of good solutions called the Pareto front (Verma et Snasel, 2021; Chakraborti et al., 2009).

4.2 Pareto approach

The Pareto scientific methodology, named after Italian economist Vilfredo Pareto, enables the identification of optimal solutions for multi-objective optimization problems. Represented by a Pareto front or curve, this approach highlights a set of "efficient" or "non-dominated" solutions where improving one objective compromises another. The Pareto method is valuable in scientific and technical contexts, balancing trade-offs between conflicting goals, such as cost versus performance or efficiency versus sustainability. Visualizations of the Pareto front, as seen in works like Deb's (2001), help researchers and engineers understand trade-offs in complex decision-making by illustrating the range of optimal solutions (Baadache et al., 2025).

4.3 Mathematical formulation of the optimization problem

Objective Function:

- Maximize the longitudinal Young's modulus (stiffness).
- Minimize von-Mises stress.

Designs variables :

- Ply angles: $(-90^\circ \leq \theta \leq 90^\circ)$.
- Ply materials: HS-Carbon/Epoxy (CF-EP), E-Glass/Epoxy (EG-EP), S-Glass/Epoxy (SG-EP).
- Number of plies: Between 6 and 12.

Constraints :

- Tsai-Wu failure index : $FI \leq 0,7$.
- 25% of the plies must be HS-Carbon/Epoxy (CF-EP).
- HS-Carbon/Epoxy (CF-EP) plies must be placed at the center of the laminate.
- All three materials (CF-EP, EG-EP and SG-EP) must be present in the laminate.

The MOGA method (Multi-Objective Genetic Algorithm) was used to optimize a hybrid composite laminate under tensile and compressive loads, maximizing the longitudinal Young's modulus E_x and minimizing the maximum von-Mises stress. Three design variables were considered: the number of plies, the ply orientation angles, and the ply materials (E-Glass/epoxy, S-Glass/epoxy and HS-Carbon /epoxy). The optimization required a maximum Tsai-Wu failure index of 0.7 for each ply, with 25% of the plies being HS-Carbon/epoxy (CF-EP), CF-EP plies positioned at the center of the laminate, and all three materials (CF-EP, EG-EP, and SG-EP) included in the laminate.

The geometric properties of the composite plate, specifically a length of 200 mm, a width of 100 mm, and a total thickness of 3 mm, were defined. Axial and biaxial tensile and compressive loads of 6000 N were applied in the longitudinal direction (axial) and in both directions (biaxial) separately, with load ratios of 0.5, 1, and 2. The laminate parameters, including ply orientation angles $(-90^\circ \leq \theta \leq 90^\circ)$, materials (E-Glass/epoxy, S-Glass/epoxy and HS-Carbon /epoxy), and number of plies (6 to 12), were set in the program. A multi-objective optimization was then performed using MATLAB's genetic algorithm ('gamultiobj').

The first step was to set up the MOGA algorithm parameters. An initial population of 1000 individuals was defined, with a maximum of 800 generations. Additionally, a second population of 2000 individuals was used, with a maximum of 1600 generations. A Pareto fraction was set to retain optimal solutions showing trade-offs between objectives. A crossover rate of 85% was chosen to promote exploration of new solutions, and an adaptive mutation function was used to maintain solution diversity. The program displays progress at each iteration, showing the best objective values.

The optimization produced a Pareto front, highlighting the trade-offs between the longitudinal Young's modulus E_x and the maximum von-Mises stress. An optimal solution was extracted, describing the laminate configuration (number of plies, orientation angles, and materials). For this solution, mechanical properties such as stresses and strains under tensile and compressive, as well as the maximum Tsai-Wu failure index, were calculated and displayed. The results also include the global Young's modulus and the maximum von-Mises stress. Details of the solution, including the ply sequence, angles, materials, and performance under tensile and compressive, are presented in Table 2 and Table 3.

5. Finite Element Analysis

Finite element analysis (FEA) allows modeling composite materials using various simulation tools. ANSYS offers several options for composite material modeling, including different simulation capabilities. ANSYS ACP, a module for creating composite laminates, simplifies defining the required thickness and stacking sequences. This module includes a layer thickness editor, a stacking sequence editor, a layer arrangement modeling tool, and a failure criteria analysis for each layer. **Fig. 2** illustrates the approach for the finite element simulation of hybrid composite laminates. In this study, the modeling of composite layers made of CF-EP, EG-EP, and SG-EP was performed using ANSYS ACP. This tool enabled the design of composite layers by specifying ply thickness and fiber orientation according to desired specifications. The next step involved laminating the hybrid composite material. In ANSYS ACP, composite material modeling is performed layer by layer, with a total laminate thickness set to 3 mm. The process began in the ACP (Pre) module with the creation of a sketch of the geometric shape, followed by a refinement of the structure using an appropriate mesh. Fiber orientations and the stacking sequence were defined using the "stackup" command. Each layer was specified with distinct materials, such as SG-EP (S-Glass/epoxy), CF-EP (HS-carbon/epoxy), and EG-EP (E-Glass/epoxy), with their mechanical properties, including elastic moduli, Poisson's ratios, and tensile strength, listed in **Table 1**. Once the geometric model and layer properties were established, finite element simulations were conducted in the "Static Structural" module of ANSYS. In the "Static Structural" module, boundary

conditions and loads were then applied as indicated in **Fig. 5**. After execution, the simulation results are displayed, including von-Mises stresses, deformations, displacements, and more. The Tsai-Wu failure index for the laminate and/or each ply is displayed in the ACP (Post) module.

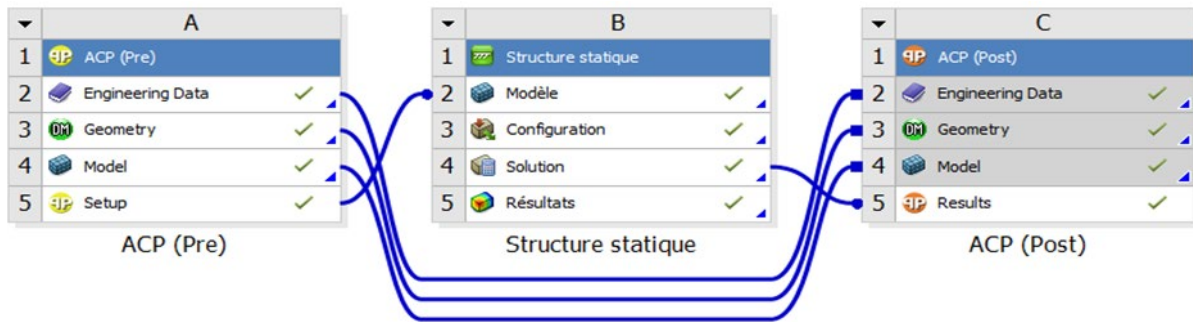


Fig. 2. Project schematic for the FEA simulation of hybrid composite laminated

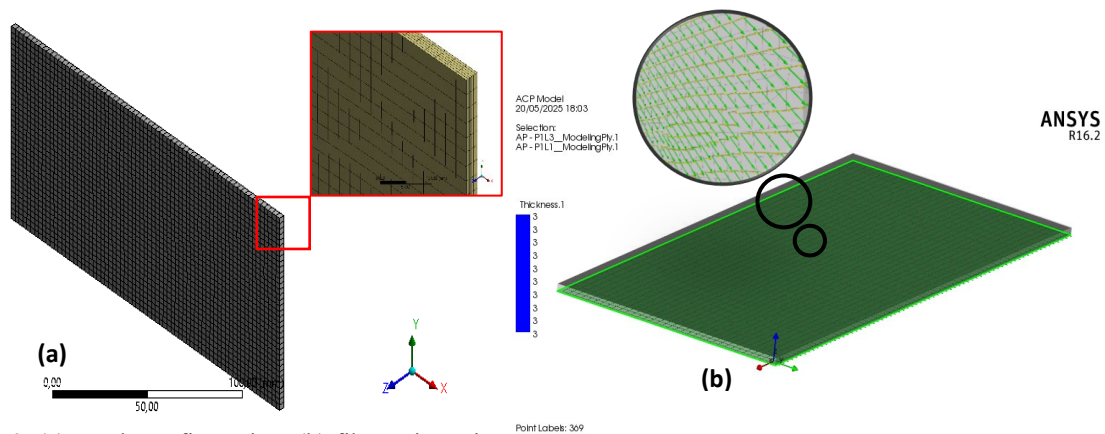


Fig. 3. (a) Mesh configuration, (b) fiber orientations in the ACP module for the hybrid composite plate.

5.1 Mesh independence

Under tensile loading, a refined mesh with an element size of 3 mm, corresponding to 22190 elements, stabilizes the von-Mises stresses at a value of 31.686 MPa, as illustrated in the provided **Fig. 4**. This element size was chosen because it marks the point where convergence is achieved, minimizing discretization errors while optimizing computational time for maximum efficiency. **Fig. 3** show the mesh structure and the fiber orientations, obtained in the ACP module.

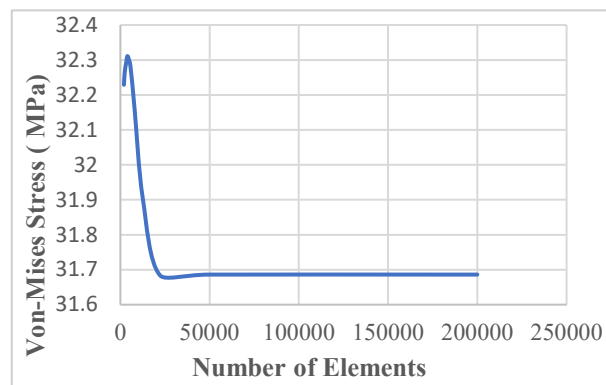


Fig. 4. Convergence of von-Mises Stress as a Function of the Number of Elements

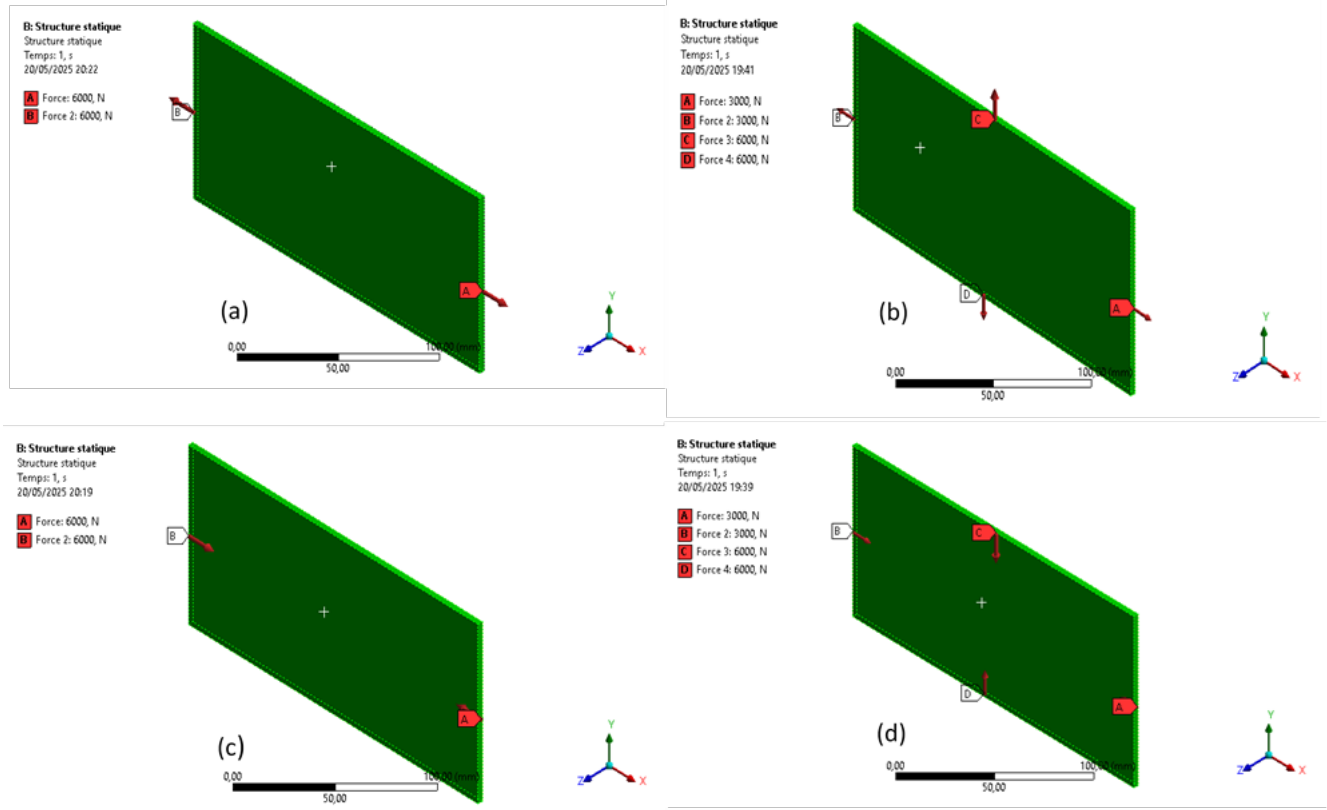


Fig. 5. Boundary conditions and applied loads: (a) axial traction, (b) biaxial traction, (c) axial compressive, (d) biaxial compressive

6. Results and discussion

6.1 Optimization and finite element analysis results

In this section, the tensile and compressive optimization results of hybrid composite laminates and their properties, obtained through a genetic algorithm implemented in MATLAB, are compared with those simulated using the finite element method (FEM), with thoroughly detailed discussions.

6.1.1 Multi-objective genetic algorithm results

6.1.1.1 Tensile optimization results

The tensile optimization results of hybrid composite laminates and their properties, obtained through a genetic algorithm for axial and biaxial loading, are listed in **Table 2**. A first run of the optimization program, axial loading with an initial population of 1000 individuals and a maximum of 800 generations, yielded a 10-layer hybrid laminate configuration with the stacking sequence $[-5_{2SG-EP}/0_{SG-EP}/0_{4CF-EP}/5_{EG-EP}/5_{2SG-EP}]$, exhibiting a maximum von-Mises stress of 30.61 MPa, a longitudinal Young's modulus E_x of 77.438 GPa, and a Tsai-Wu failure index of 0.033. A second run, with an initial population of 2000 individuals and a maximum of 1600 generations, produced the same laminate configuration with identical properties. Consequently, the first configuration, with 1000 individuals and 800 generations, was selected to optimize computational time. Subsequently, running the optimization program for biaxial loading with a force ratio of 0.5 (defined as $R = F_y/F_x$) resulted in a 10-layer hybrid laminate configuration with the stacking sequence $[0_{2SG-EP}/-90_{EG-EP}/0_{4CF-EP}/0_{SG-EP}/0_{2EG-EP}]$, showing a maximum von-Mises stress of 29.67 MPa, a longitudinal Young's modulus E_x of 73.489 GPa, and a Tsai-Wu failure index of 0.198. For a force ratio of 1, an 8-layer hybrid laminate configuration was obtained, with the stacking sequence $[90_{SG-EP}/0_{SG-EP}/-45_{EG-EP}/45_{CF-EP}/0_{CF-EP}/-45_{EG-EP}/0_{SG-EP}/-90_{EG-EP}]$, characterized by a maximum von-Mises stress of 37.98 MPa, a longitudinal Young's modulus E_x of 30.362 GPa, and a Tsai-Wu failure index of 0.192. Finally, for a force ratio of 2, a 6-layer hybrid laminate configuration was achieved, with the stacking sequence $[-90_{EG-EP}/90_{EG-EP}/0_{2CF-EP}/90_{2SG-EP}]$, presenting a maximum von-Mises stress of 26.79 MPa, a longitudinal Young's modulus E_x of 47.946 GPa, and a Tsai-Wu failure index of 0.189.

Table 2. Presentation of Tensile Loading Optimization Results.

Tensile loads	Stacking sequence	Von-Mises stress (MPa)	Young's Modul (GPa)	Tsai-Wu index
Tensile axial	$[-5_{2SG-EP}/0_{SG-EP}/0_{4CF-EP}/5_{EG-EP}/5_{2SG-EP}]$	30.61	77.438	0.033
Tensile biaxial $R=0.5$	$[0_{2SG-EP}/-90_{EG-EP}/0_{4CF-EP}/0_{SG-EP}/0_{2EG-EP}]$	29.67	73.489	0.198
Tensile biaxial $R=1$	$[90_{SG-EP}/0_{SG-EP}/-45_{EG-EP}/45_{CF-EP}/0_{CF-EP}/-45_{EG-EP}/0_{SG-EP}/-90_{EG-EP}]$	37.98	30.362	0.192
Tensile biaxial $R=2$	$[-90_{EG-EP}/90_{EG-EP}/0_{2CF-EP}/90_{2SG-EP}]$	26.79	47.946	0.189

6.1.1.2 Compressive optimization results

In this paragraph, we present the results of compressive optimization, listed in **Table 3**. For compressive under axial loading, a 6-layer hybrid laminate configuration was obtained, with the stacking sequence $[-90_{SG-EP}/-90_{EG-EP}/-90_{2CF-EP}/-90_{2EG-EP}]$, characterized by a maximum von-Mises stress of 21.85 MPa, a longitudinal Young's modulus E_x of 11.077 GPa, and a Tsai-Wu failure index of 0.178. For compressive under biaxial loading, three configurations were generated. With a force ratio of 0.5 (defined as $R = F_y/F_x$), an 8-layer hybrid laminate configuration was obtained, with the stacking sequence $[29_{EG-EP}/-13_{SG-EP}/-15_{EG-EP}/-3_{CF-EP}/-6_{CF-EP}/3_{SG-EP}/22_{SG-EP}/-18_{EG-EP}]$, exhibiting a maximum von-Mises stress of 33.566 MPa, a longitudinal Young's modulus E_x of 50.52 GPa, and a Tsai-Wu failure index of 0.107. For a force ratio of 1, a 6-layer hybrid laminate configuration was generated, with the stacking sequence $[3_{SG-EP}/-4_{EG-EP}/0_{2CF-EP}/-6_{SG-EP}/4_{SG-EP}]$, characterized by a maximum von-Mises stress of 25.57 MPa, a longitudinal Young's modulus E_x of 70.405 GPa, and a Tsai-Wu failure index of 0.092. Finally, for a force ratio of 2, a 8-layer hybrid laminate configuration was obtained, with the stacking sequence $[-50_{SG-EP}/-50_{EG-EP}/-45_{EG-EP}/-45_{2CF-EP}/-40_{EG-EP}/-30_{SG-EP}/-25_{EG-EP}]$, presenting a maximum von-Mises stress of 18.82 MPa, a longitudinal Young's modulus E_x of 17.657 GPa, and a Tsai-Wu failure index of 0.099.

Table 3. Presentation of Compressive Loading Optimization Results.

Compressive loads	Stacking sequence	Von-Mises stress (MPa)	Young's Modul (GPa)	Tsai-Wu index
Compressive axial	$[-90_{SG-EP}/-90_{EG-EP}/-90_{2CF-EP}/-90_{2EG-EP}]$	21.85	11.077	0.178
Compressive biaxial $R=0.5$	$[29_{EG-EP}/-13_{SG-EP}/-15_{EG-EP}/-3_{CF-EP}/-6_{CF-EP}/3_{SG-EP}/22_{SG-EP}/-18_{EG-EP}]$	33.566	50.52	0.107
Compressive biaxial $R=1$	$[3_{SG-EP}/-4_{EG-EP}/0_{2CF-EP}/-6_{SG-EP}/4_{SG-EP}]$	25.57	70.405	0.092
Compressive biaxial $R=2$	$[-50_{SG-EP}/-50_{EG-EP}/-45_{EG-EP}/-45_{2CF-EP}/-40_{EG-EP}/-30_{SG-EP}/-25_{EG-EP}]$	18.82	17.657	0.099

The optimization results presented above, obtained through a multi-objective genetic algorithm, highlight the performance of hybrid composite laminates under various tensile and compressive loadings. These analyses enable the identification of optimal configurations suited to the studied mechanical conditions. The following section presents the results obtained by the finite element method (FEM), providing a direct comparison with the optimization results to assess their consistency and reliability.

6.2 Finite element analysis results

6.2.1 Numerical validation

To validate the numerical model, this study's results were compared with experimental and numerical data from Hatti, Prashant S., et al. (2022). The theoretical results were calculated using Classical Laminated Theory (CLT). Hatti, Prashant S et al. (2022) conducted a tensile study using the finite element method with ANSYS Workbench and the ACP module on composite laminates made of E-glass /epoxy (EG-EP) plies. They compared three samples with different fiber orientations, namely $[90_{10}]$, $[45_{10}]$, and $[30_{10}]$. The tensile test was performed on samples measuring 250 mm in length and 25 mm in width. The composite plate consisted of ten EG-EP plies, each with a thickness of 0.25 mm, resulting in a total thickness of 2.5 mm. A tensile load was applied to two opposite sides of the plate in the X direction, with values of 5903.8 N, 5913.60 N, and 6149 N for the laminates $[90_{10}]$, $[45_{10}]$, and $[30_{10}]$, respectively. To compare our results and validate our calculation model (CLPT), we applied the same boundary conditions as those used in the study by Hatti et al. (2022). To obtain results identical to those of the study conducted by Hatti et al. (2022), the mesh structure of the composite plate was generated using Solid 185 (3D) elements. Convergence analyses were conducted to identify the optimal element size for accurate stress calculations. A total of 62500 Solid 185 elements were employed in the 3D finite element model of the composite plate, as shown by Hatti, Prashant S et al. (2022). **Table 4** presents a comparison between our results and those of that study.

Table 4 shows the variation in stress values (in MPa) of the composite for different fiber orientations. Specifically, the highest stress value was recorded in the composite laminates configured with a $[30_{10}]$ fiber orientation, reaching (98.384 MPa), while the minimum stress was obtained for the laminates with the $[90_{10}]$ orientation (94.461 MPa). The current predictions were found to be very close to the published results. As noted by Prashant S. Hatti et al. (2022), a slight difference was observed between the experimental and numerical results, attributed to manufacturing imperfections and experimental uncertainties. In contrast, the numerical results (FEM) were in perfect agreement, at 100%, with the theoretical results.

Table 4. Comparison Table for Tensile Test.

Study of Prashant S. Hatti et al. (2022)					This study	
Sl.N ^o	θ (In degrees)	Load(N)	Von-Mises stress Experimental (MPa)	Von-Mises stress FEA (MPa)	Von-Mises stress MOGA (MPa)	Von-Mises stress FEA (MPa)
1	90	5903	97.4	95.25	94.461	94.461
2	45	5913	101.5	99.19	94.618	94.618
3	30	6149	99.85	98.38	98.384	98.384

The simulation aimed at calculating the equivalent von-Mises stress, the longitudinal Young’s modulus E_x , and the Tsai-Wu failure index for the configurations of hybrid composite laminates obtained via a multi-objective genetic algorithm was performed using the ANSYS Workbench 16.2 finite element solver. This analysis provided essential information on the mechanical behavior of the hybrid composite laminates. **Fig. 6** and **Fig. 7** illustrate the distribution of von-Mises stresses under axial and biaxial tensile and compressive, produced by the simulation with a mesh size of 3 mm, as detailed in section 5.1. (Mesh Independence). For axial tensile, the hybrid laminate with the stacking sequence $[-5_{2SG-EP}/0_{SG-EP}/0_{4CF-EP}/5_{EG-EP}/5_{2SG-EP}]$ exhibiting a von-Mises stress of 31.686 MPa, a longitudinal Young’s modulus E_x of 78.738 GPa, and a Tsai-Wu index of 0.023 shows in **Fig. 9-a**. For axial compressive, the laminate with the stacking sequence $[-90_{SG-EP}/-90_{EG-EP}/-90_{2CF-EP}/-90_{2EG-EP}]$ shows a von-Mises stress of 21.859 MPa, a longitudinal Young’s modulus E_x of 9.32 GPa, and a Tsai-Wu index of 0.197 shows in **Fig. 9-b**.

For biaxial loadings, the simulations of tensile and compressive were also performed with ANSYS Workbench 16.2. For a force ratio $R = F_y/F_x$ equal to 0.5, the stacking $[0_{2SG-EP}/-90_{EG-EP}/0_{4CF-EP}/0_{SG-EP}/0_{2EG-EP}]$ in biaxial tensile shows a von-Mises stress of 31.391 MPa, a longitudinal Young’s modulus E_x of 81.926 GPa, and a Tsai-Wu index of 0.167, while the sequence $[29_{EG-EP}/-13_{SG-EP}/-15_{EG-EP}/-3_{CF-EP}/-6_{CF-EP}/3_{SG-EP}/22_{SG-EP}/-18_{EG-EP}]$ in biaxial compressive presents a von-Mises stress of 34.89 MPa, a longitudinal Young’s modulus E_x of 50.102 GPa, and a Tsai-Wu index of 0.044. For $R = 1$, the sequence $[90_{SG-EP}/0_{SG-EP}/-45_{EG-EP}/45_{CF-EP}/0_{CF-EP}/-45_{EG-EP}/0_{SG-EP}/-90_{EG-EP}]$ in biaxial tensile indicates a von-Mises stress of 37.55 MPa, a longitudinal Young’s modulus E_x of 31.112 GPa, and a Tsai-Wu index of 0.298, while the sequence $[3_{SG-EP}/-4_{EG-EP}/0_{2CF-EP}/-6_{SG-EP}/4_{SG-EP}]$ in biaxial compressive displays a von-Mises stress of 27.926 MPa, a longitudinal Young’s modulus E_x of 73.79 GPa, and a Tsai-Wu index of 0.096. Finally, for $R = 2$, the sequence $[-90_{EG-EP}/90_{EG-EP}/0_{2CF-EP}/90_{2SG-EP}]$ in biaxial tensile reveals a von-Mises stress of 23.848 MPa, a longitudinal Young’s modulus E_x of 36.282 GPa, and a Tsai-Wu index of 0.204, while the sequence $[-50_{SG-EP}/-50_{EG-EP}/-45_{EG-EP}/-45_{2CF-EP}/-40_{EG-EP}/-30_{SG-EP}/-25_{EG-EP}]$ in biaxial compressive shows a von-Mises stress of 14.168 MPa, a longitudinal Young’s modulus E_x of 23.06 GPa, and a Tsai-Wu index of 0.091. The values of the longitudinal Young’s modulus (E_x) for each laminate were calculated from the stress-strain curves illustrated in **Fig. 8**, applying Hooke’s law ($E_x = \sigma/\epsilon$, or $E_x = \Delta\sigma/\Delta\epsilon$). These calculations correspond to the stacking sequences associated with their loading conditions, whether tensile or compressive, and axial or biaxial.

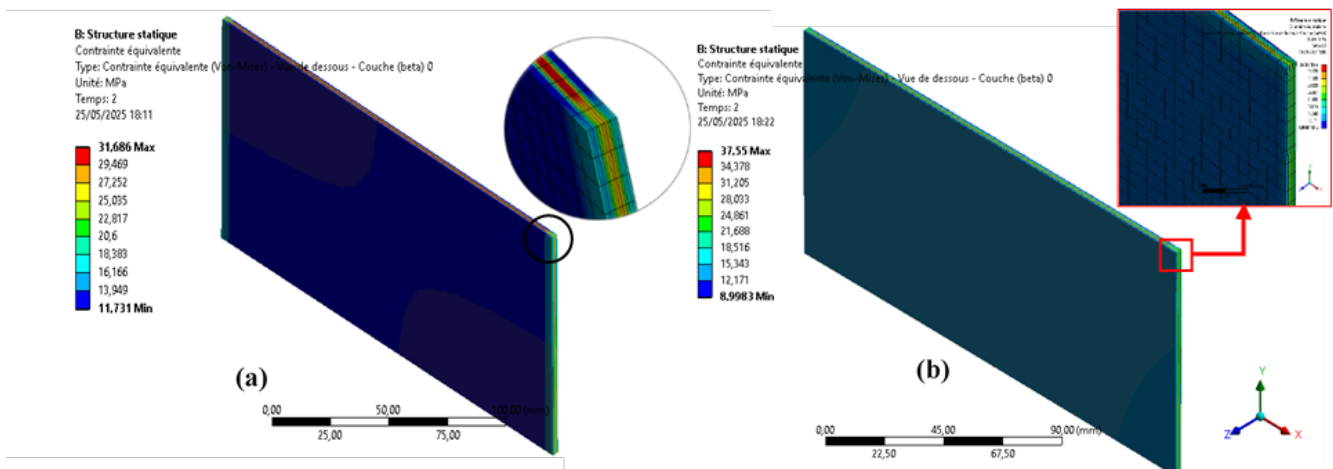


Fig. 6. The von-Mises stress, **(a)** von-Mises stress of the hybrid composite plate $[-5_{2SG-EP}/0_{SG-EP}/0_{4CF-EP}/5_{EG-EP}/5_{2SG-EP}]$ subjected to axial tensile load. **(b)** von-Mises stress of the hybrid composite plate $[90_{SG-EP}/0_{SG-EP}/-45_{EG-EP}/45_{CF-EP}/0_{CF-EP}/-45_{EG-EP}/0_{SG-EP}/-90_{EG-EP}]$ subjected to biaxial tensile load for $R=1$.

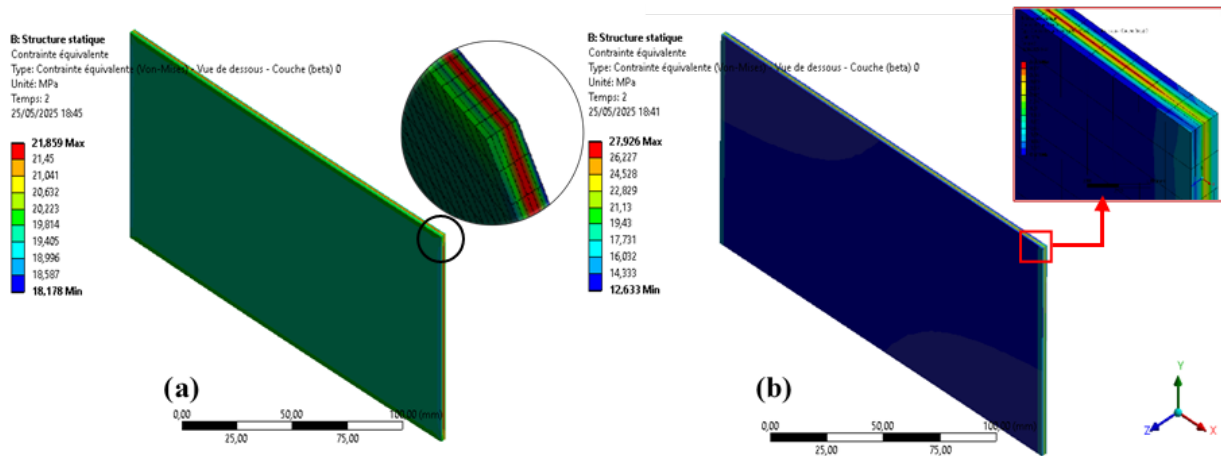


Fig. 7. The von-Mises stress, **(a)** von-Mises stress of the hybrid composite plate $[-90_{SG-EP}/-90_{EG-EP}/-90_{2CF-EP}/-90_{2EG-EP}]$ subjected to axial compressive load. **(b)** von-Mises stress of the hybrid composite plate $[3_{SG-EP}/4_{EG-EP}/0_{2CF-EP}/-6_{SG-EP}/4_{SG-EP}]$ subjected to biaxial compressive load for $R=1$.

Following the presentation of our study’s results on the mechanical performance of hybrid composite laminates under tensile and compressive, we now proceed to the discussion of these finding

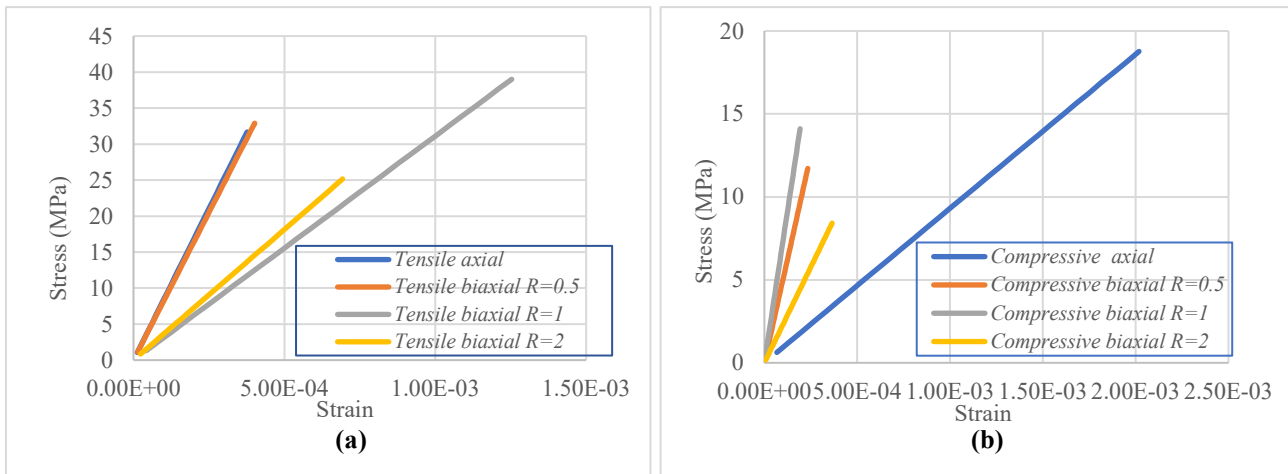


Fig. 8. (a): Stress vs strain of different tensile loads, **(b):** Stress vs strain of different compressive loads

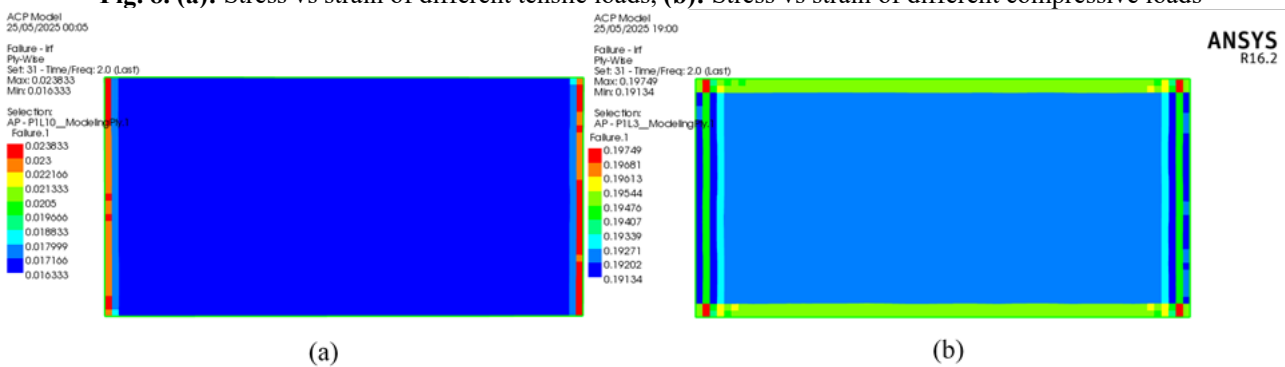


Fig. 9. Tsai-Wu failure indices, **(a)** failure indices of ply 10 for the hybrid composite plate $[-52_{SG-EP}/0_{SG-EP}/0_{4CF-EP}/5_{EG-EP}/52_{SG-EP}]$ subjected to axial tensile load. **(b)** failure indices of ply 3 for the hybrid composite plate $[-90_{SG-EP}/-90_{EG-EP}/-90_{2CF-EP}/-90_{2EG-EP}]$ subjected to axial compressive load.

6.3 Discussion

As mentioned by NOMAN, Abdulla Al et al. (2023), fiber orientation plays a crucial role in the mechanical properties of composite laminates. Moreover, the material of the fibers directly influences their mechanical characteristics. In the fields of automotive, aeronautics, and civil engineering, some mechanical parts are subjected to axial or biaxial tensile forces, while

others undergo axial or biaxial compressive forces. The placement of carbon fibers in the middle of hybrid laminates results in lower stress for the laminate compared to their position on the outside, as demonstrated in the study by KUMAR, Kaushlendra, et al. (2024). Through multi-objective optimization, our study enables the selection of the optimal fiber orientation as well as the type of fiber material based on specific needs and the loads to which the part will be exposed. In general, for parts subjected to purely axial tensile forces, the fiber orientation ranges between 0° and 5°. The study by ANTO, Anik Das et al. (2019) has demonstrated that laminates oriented at 0° exhibit stability under tensile loads, with particularly high rigidity values. Tables 2 and 3 present the optimal fiber orientation for each type of loading, as well as the stacking sequence of materials. Finite element method simulations, conducted using the ANSYS Workbench software, have been performed with the same fiber orientations and loading conditions. These simulations have led to results consistent with those obtained through optimization, particularly in terms of von-Mises stress, Young’s modulus, and Tsai-Wu index. The results of each type of loading obtained by MOGA are compared with those of FEM in Fig. 10, Fig. 11, and Fig. 12.

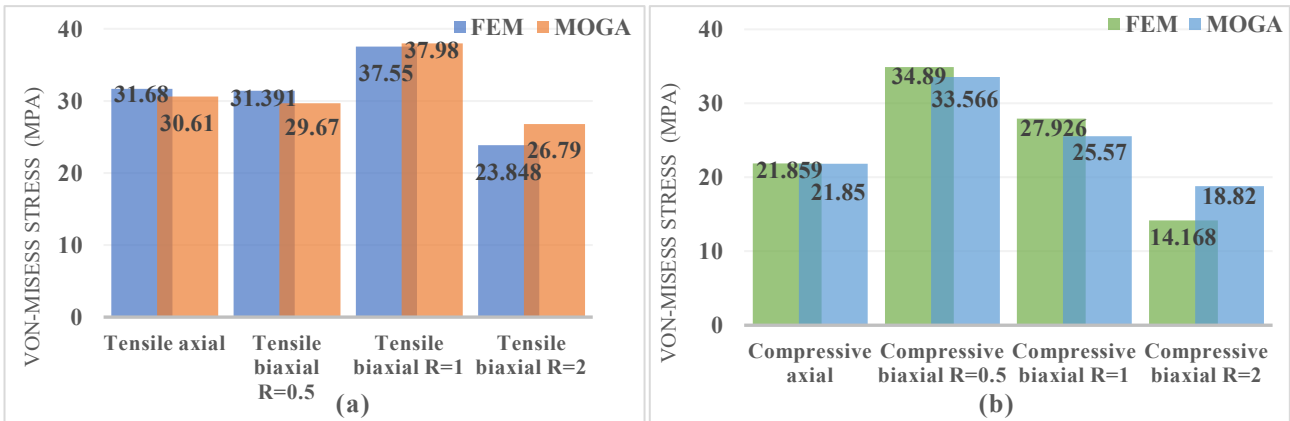


Fig. 10. Comparison of von-Mises stress between FEM and MOGA. (a) von-Mises stress for Tensile Load Conditions, (b) von-Mises stress for Compressive Load Conditions.

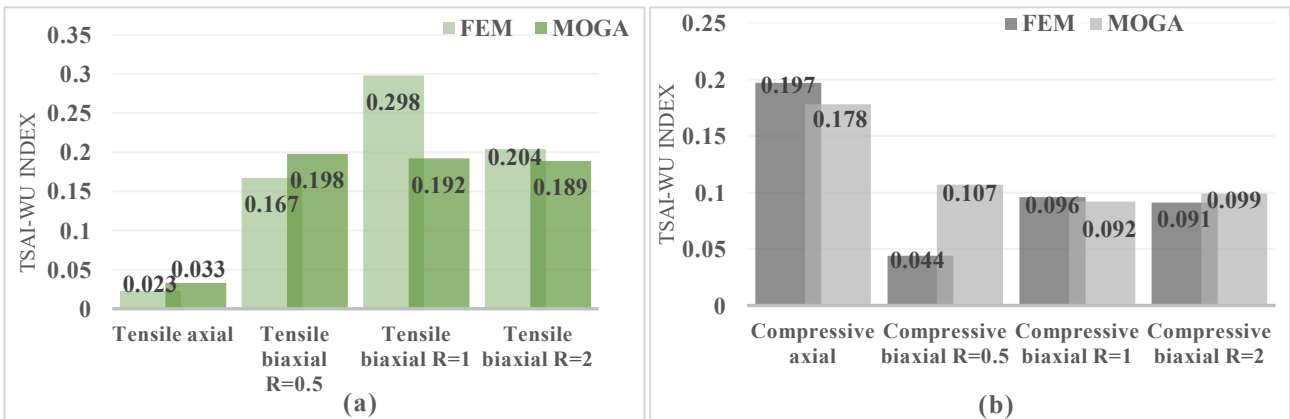


Fig. 11. Comparison of Young’s Modul between FEM and MOGA. (a) Young’s Modul for Tensile Load Conditions, (b) Young’s Modul for Compressive Load Conditions.

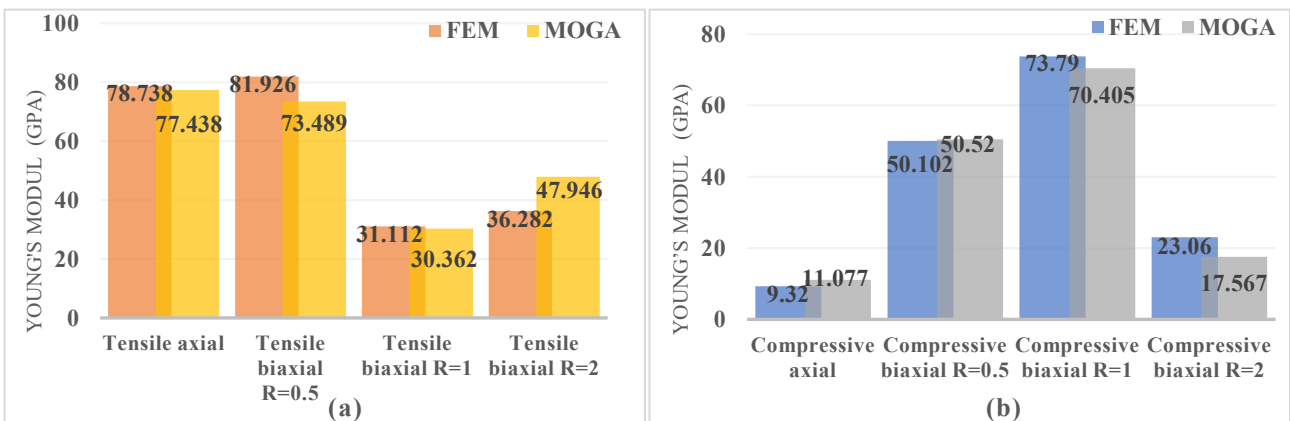


Fig. 12. Comparison of Tsai-Wu index between FEM and MOGA. (a) Tsai-Wu index for Tensile Load Conditions, (b) Tsai-Wu index for Compressive Load Conditions.

The results put in evidence the notable influence of the fiber orientation and the stacking sequence of materials (CF-EP, EG-EP, SG-EP) on the mechanical properties of hybrid composite laminates. The hybrid laminate with the stacking sequence $[-5_{2SG-EP}/0_{SG-EP}/0_{4CF-EP}/5_{EG-EP}/5_{2SG-EP}]$ shows a distinct behavior under an axial tensile load: the orientations at 0° and 5° offer high strength, low stress, and a very low Tsai-Wu failure index, thanks to the central position of the carbon fibers (CF-EP). These properties, obtained by MOGA and compared with those of FEM, show remarkable consistency, with percentage errors of 1.63% for the von-Mises stress, 4.06% for the longitudinal Young's modulus, and 30.3% for the Tsai-Wu index. The results of the entire study are detailed in **Fig. 10**, **Fig. 11**, and **Fig. 12**. For axial compressive, the stacking sequence $[-90_{SG-EP}/-90_{EG-EP}/-90_{2CF-EP}/-90_{2EG-EP}]$ presents percentage errors of 0.04%, 15.86%, and 9.64%, respectively for the von-Mises stress, the longitudinal Young's modulus, and the Tsai-Wu index.

In contrast, the hybrid laminates under biaxial tensile, with sequentially varying fiber orientations, illustrate compromises between strength and ductility. The stacking sequences for the force ratios 0.5, 1, and 2, namely $[0_{2SG-EP}/-90_{EG-EP}/0_{4CF-EP}/0_{SG-EP}/0_{2EG-EP}]$, $[90_{SG-EP}/0_{SG-EP}/-45_{EG-EP}/45_{CF-EP}/0_{CF-EP}/-45_{EG-EP}/0_{SG-EP}/-90_{EG-EP}]$ and $[-90_{EG-EP}/90_{EG-EP}/0_{2CF-EP}/90_{2SG-EP}]$, show percentage errors of: (5.48%, 1.13%, 10.98%) for the von-Mises stress, (10.3%, 2.41%, 24.36%) for the longitudinal Young's modulus, and (15.65%, 33.57%, 7.35%) for the Tsai-Wu index. Finally for biaxial compressive, the stacking sequences $[29_{EG-EP}/-13_{SG-EP}/-15_{EG-EP}/-3_{CF-EP}/-6_{CF-EP}/3_{SG-EP}/22_{SG-EP}/-18_{EG-EP}]$, $[3_{SG-EP}/-4_{EG-EP}/0_{2CF-EP}/-6_{SG-EP}/4_{SG-EP}]$ and $[-50_{SG-EP}/-50_{EG-EP}/-45_{EG-EP}/-45_{2CF-EP}/-40_{EG-EP}/-30_{SG-EP}/-25_{EG-EP}]$ for the force ratios 0.5, 1, and 2, display percentage errors of: (3.79%, 8.43%, 24.71%) for the von-Mises stress, (0.82%, 4.58%, 23.4%) for the longitudinal Young's modulus, and (58.87%, 4.16%, 8.08%) for the Tsai-Wu index. The FEM and MOGA methods are very useful for studying hybrid composite laminates. They provide very close results, with small errors for the von-Mises stress: only 1.63% in axial tensile and 0.04% in axial compressive, which proves they predict stresses well. The simulations performed using ANSYS Workbench and the genetic algorithm implemented in MATLAB enable a robust analysis under various loadings, including axial and biaxial conditions ($R=0.5, 1, 2$), offering a solid foundation for optimization. These tools help to better understand the behaviors of laminates based on their orientations and sequences.

7. Conclusion

The present study utilized a multi-objective genetic algorithm (MOGA) implemented in MATLAB to determine the optimal configuration of a hybrid composite laminate, including the number of layers, fiber orientation, and material sequence, with a failure condition ≤ 0.7 , which constitutes an effective strategy. This allows navigation through the complexities of trade-offs between the stiffness, von-Mises stress, and Tsai-Wu failure index of a hybrid composite laminate subjected to axial and biaxial tensile and compressive loads. The design variable limits were chosen to ensure the desired strength of the hybrid composite laminate. Based on the results obtained using the genetic algorithm, a comparison with the finite element method (FEM) was conducted, demonstrating crucial consistency of the results, and the optimized parameters were identified. From this study, the following conclusions can be drawn:

- Increasing the number of layers and optimizing fiber orientation improve stiffness and reduce the Tsai-Wu failure index, while controlling von-Mises stresses.
- The use of MOGA in the design of hybrid composite laminates has proven to be a reliable tool, enabling the simultaneous optimization of multiple mechanical properties.
- The comparison with the finite element method (FEM) validated the accuracy of the results obtained by MOGA, confirming the effectiveness of this integrated approach for the optimization of hybrid composite laminates.
- The integration of the three materials – HS-Carbon /Epoxy (CF-EP), E-Glass/Epoxy (EG-EP), and S-Glass/Epoxy (SG-EP) – into a single optimization problem for a laminate, in order to optimize their best mechanical characteristics, has been successfully achieved, demonstrating the feasibility and effectiveness of this integrated approach.

References

- Albadr, M. A., Tiun, S., Ayob, M., & Al-Dhief, F. T. (2020). Genetic algorithm based on natural selection theory for optimization problems. *Symmetry*, 12(11), 1758. <https://doi.org/10.3390/sym12111758>
- Anam, S. (2019). Parameters estimation of enzymatic reaction model for biodiesel synthesis by using real coded genetic algorithm with some crossover operations. *IOP Conference Series: Materials Science and Engineering*, 546, 052006. <https://doi.org/10.1088/1757-899X/546/5/052006>
- ANSYS Inc. (2015). *ANSYS user's manual* (Version 16.2) [Computer software].
- Anto, A. D., Mia, S., & Hasib, M. A. (2019). The influence of number and orientation of ply on tensile properties of hybrid composites. *Journal of Physics: Materials*, 2(2), 025002. <https://doi.org/10.1088/2515-7639/aaff7a>
- Aymerich, F., & Serra, M. (2008). Optimization of laminate stacking sequence for maximum buckling load using the ant colony optimization (ACO) metaheuristic. *Composites Part A: Applied Science and Manufacturing*, 39(2), 262–272. <https://doi.org/10.1016/j.compositesa.2007.10.011>

- Baadache, K., Guedouh, M. S., & Haddad, D. (2025). A multi-objective optimization of window surface and glass thickness determination for daylight factor, thermal resistance and acoustic insulation of a test room performances under an overcast sky. *Journal of Building Engineering*, *101*, 111717. <https://doi.org/10.1016/j.jobbe.2024.111717>
- Barbero, E. J., & Cortes, D. H. (2010). A mechanistic model for transverse damage initiation, evolution, and stiffness reduction in laminated composites. *Composites Part B: Engineering*, *41*(2), 124–132.
- Berthelot, J.-M. (2005). *Composite materials: Mechanical behavior and structural analysis*. Editions Tec & Doc.
- Beylergil, B. (2020). Multi-objective optimal design of hybrid composite laminates under eccentric loading. *Alexandria Engineering Journal*, *59*(6), 4969–4983. <https://doi.org/10.1016/j.aej.2020.09.015>
- Beylergil, B., Cunedioğlu, Y., & Aktaş, A. (2011). Experimental and numerical analysis of single lap composite joints with inter-adherend fibers. *Composites Part B: Engineering*, *42*(7), 1885–1896. <https://doi.org/10.1016/j.compositesb.2011.06.010>
- Bhaskar Reddy, K., Singh, N., Saluja, R. K., & Murali, G. (2023). Experimental and computational evaluation of mechanical properties of glass epoxy composite laminates at different fiber orientations. In *International Conference on Modern Research in Aerospace Engineering* (pp. 135–145). Springer Nature Singapore. https://doi.org/10.1007/978-981-97-1306-6_11
- Bugeda Castelltort, G., Lee, D. S., Morillo Carbonell, C., & Oñate, E. (2012). Multilayered composite structure design optimization using distributed/parallel multi-objective evolutionary algorithms. *Composite Structures*, *94*(3), 1156–1166. <https://doi.org/10.1016/j.compstruct.2011.10.009>
- Casavola, C., Cazzato, A., Moramarco, V., & Pappalettere, C. (2016). Orthotropic mechanical properties of fused deposition modeling parts described by classical laminate theory. *Materials & Design*, *90*, 453–458. <https://doi.org/10.1016/j.matdes.2015.11.009>
- Chakraborti, N., Sreevathsan, R., Jayakanth, R., & Chowdhury, S. (2009). Tailor-made material design: An evolutionary approach using multi-objective genetic algorithms. *Computational Materials Science*, *45*(1), 1–7. <https://doi.org/10.1016/j.commatsci.2008.03>
- Chang, N., Wang, W., Yang, W., & Wang, J. (2010). Ply stacking sequence optimization of composite laminate by permutation discrete particle swarm optimization. *Structural and Multidisciplinary Optimization*, *41*(2), 179–187. <https://doi.org/10.1007/s00158-009-0417-x>
- Daniel, I. M., & Ishai, O. (1994). *Engineering mechanics of composite materials*. Oxford University Press.
- Deb, K. (2001). *Multi-objective optimization using evolutionary algorithms*. John Wiley & Sons.
- Gdoutos, E. E. (2005). *Fracture mechanics: An introduction* (2nd ed.). Springer.
- Hatti, P. S., Somanakatti, A. B., & Sahu, D. (2022). Investigation on tensile behavior of glass-fiber reinforced polymer matrix composite with varying orientations of fibers. *Materials Today: Proceedings*, *54*, 137–140. <https://doi.org/10.1016/j.matpr.2021.08.196>
- Henrichsen, S. R. (2015). *Optimization of laminated composite structures* [Doctoral dissertation, Aalborg University]. VBN Research Database. <https://doi.org/10.5278/vbn.phd.engsci.00041>
- Huang, L., Ng, C.-T., Sheikh, A. H., & Griffith, M. C. (2017). Niching particle swarm optimization techniques for multimodal buckling maximization of composite laminates. *Applied Soft Computing*, *57*, 495–503. <https://doi.org/10.1016/j.asoc.2017.04.006>
- Hutton, D. V. (2004). *Fundamentals of finite element analysis*. McGraw-Hill.
- Hwang, M.-Y., Park, J. H., Song, J., & Kim, S.-W. (2023). Enhanced reverse-engineering method for accurately predicting lamina properties in laminated composites via combined static and dynamic finite element simulations. *Journal of Composites Science*, *7*(12), 518. <https://doi.org/10.3390/jcs7120518>
- Jones, R. M. (1999). *Mechanics of composite materials* (2nd ed.). CRC Press.
- Kaufmann, M., Zenkert, D., & Mattei, C. (2008). Cost optimization of composite aircraft structures including variable laminate qualities. *Composites Science and Technology*, *68*(13), 2748–2754. <https://doi.org/10.1016/j.compscitech.2008.05.024>
- Kaw, A. K. (2005). *Mechanics of composite materials* (2nd ed.). CRC Press.
- Kumar, K., Mishra, Y. K., Kumar, J., & Kumar, A. (2024). Exploration of stacking effects of carbon/glass fabric in polymer hybrid composites: Analysis of mechanical properties. *Discover Applied Sciences*, *6*(12), 1–14. <https://doi.org/10.1007/s42452-024-06348-5>
- Kumar, K. P. M., & Murthy, M. (2020). Studies on E-glass and S-glass hybrid polymer matrix composites. *Materials Today: Proceedings*, *24*, 1064–1076. <https://doi.org/10.1016/j.matpr.2020.04.420>
- Kumpati, R., Skarka, W., Skarka, M., & Suresh, R. (2024). Enhanced optimization of composite laminates: Multi-objective genetic algorithms with improved ply-stacking sequences. *Materials*, *17*(4), 887. <https://doi.org/10.3390/ma17040887>
- Lin, C.-C., & Lee, Y.-J. (2004). Stacking sequence optimization of laminated composite structures using genetic algorithm with local improvement. *Composite Structures*, *63*(3–4), 339–345. [https://doi.org/10.1016/S0263-8223\(03\)00182-X](https://doi.org/10.1016/S0263-8223(03)00182-X)
- Mache, A., & Deb, A. (2013). A comparative study on the axial impact performance of jute and glass fiber-based composite tubes [Technical paper]. *SAE Technical Paper Series*, 2013-01-1178. <https://doi.org/10.4271/2013-01-1178>
- Meng, M., Le, H. R., Rizvi, M. J., & Grove, S. M. (2015). 3D FEA modelling of laminated composites in bending and their failure mechanisms. *Composite Structures*, *119*, 693–708. <https://doi.org/10.1016/j.compstruct.2014.09.048>
- Merhar, M. (2020). Determination of elastic properties of beech plywood by analytical, experimental and numerical methods. *Forests*, *11*(11), 1221. <https://doi.org/10.3390/f11111221>

- Monte, S. M. C., Infante, V., Madeira, J. F. A., & Moleiro, F. (2017). Optimization of fibers orientation in a composite specimen. *Mechanics of Advanced Materials and Structures*, 24(5), 410–416. <https://doi.org/10.1080/15376494.2016.1191099>
- Noman, A. A., Shohel, S. M., Riyad, S. H., & Hasan, M. (2023). Investigate the mechanical strength of laminated composite carbon fiber with different fiber orientations by numerically using finite element analysis. *Materials Today: Proceedings*. Advance online publication. <https://doi.org/10.1016/j.matpr.2023.02.132>
- Riccio, A., Di Caprio, F., Tsai, S. W., & Palumbo, C. (2024). Optimization of composite aeronautical components by re-designing with double-double laminates. *Aerospace Science and Technology*, 151, 109304. <https://doi.org/10.1016/j.ast.2024.109304>
- Sabau, E., Popescu, A., & Vilau, C. (2017). Mechanical behavior of composite materials using the finite element analysis. *MATEC Web of Conferences*, 137, 08006. <https://doi.org/10.1051/mateconf/201713708006>
- Satkar, A. R., Mache, A., & Kulkarni, A. (2022). Numerical investigation on perforation resistance of glass-carbon/epoxy hybrid composite laminate under ballistic impact. *Materials Today: Proceedings*, 59, 734–741. <https://doi.org/10.1016/j.matpr.2021.12.464>
- Shaikh, A. A., Pradhan, A. A., Kotasthane, A. M., & Burande, S. W. (2022). Comparative analysis of basalt/E-glass/S2-fibreglass-carbon fiber reinforced epoxy laminates using finite element method. *Materials Today: Proceedings*, 63, 630–638. <https://doi.org/10.1016/j.matpr.2022.04.385>
- Shokrieh, M. M., & Lessard, L. B. (2000). Progressive fatigue damage modeling of composite materials, Part II: Material characterization and model verification. *Journal of Composite Materials*, 34(13), 1081–1116. <https://doi.org/10.1177/002199830003401302>
- Stosiak, M., Lubecki, M., & Karpenko, M. (2025). Designing a composite hydraulic cylinder using genetic algorithms. *Actuators*, 14(2), 77. <https://doi.org/10.3390/act14020077>
- Suresh, S., Sujit, P. B., & Rao, A. K. (2007). Particle swarm optimization approach for multi-objective composite box-beam design. *Composite Structures*, 81(4), 598–605. <https://doi.org/10.1016/j.compstruct.2006.10.008>
- Verma, S., Pant, M., & Snasel, V. (2021). A comprehensive review on NSGA-II for multi-objective combinatorial optimization problems. *IEEE Access*, 9, 57757–57791. <https://doi.org/10.1109/ACCESS.2021.3070634>
- Vlase, S., Teodorescu-Draghicescu, H., Călin, M. R., & Serbina, L. (2011). Simulation of the elastic properties of some fibre-reinforced composite laminates under off-axis loading system. *Optoelectronics and Advanced Materials – Rapid Communications*, 5(4), 424–429.
- Wang, X., Cai, D., Silberschmidt, V. V., & Chen, S. (2019). Tensile properties of 3D multi-layer wrapping braided composite: Progressive damage analysis. *Composites Part B: Engineering*, 176, 107334. <https://doi.org/10.1016/j.compositesb.2019.107334>
- Yibre, A. M., Koçer, B., Esleman, E. A., & Ülker, M. (2020). Weight optimization of hybrid composite laminate using learning-oriented artificial algae algorithm. *SN Applied Sciences*, 2, 1–13. <https://doi.org/10.1007/s42452-020-3126-0>
- Zhang, W., Tang, W. Y., Pu, Y. C., & Chen, X. Q. (2011). Ultimate strength analysis of ship hulls of continuous basalt fiber composite materials. *Advanced Materials Research*, 150, 736–740. <https://doi.org/10.4028/www.scientific.net/AMR.150-151.736>
- Zhang, Z., Liao, C., Chai, H., & Wu, H. (2021). Multi-objective optimization of controllable configurations for bistable laminates using NSGA-II. *Composite Structures*, 266, 113764. <https://doi.org/10.1016/j.compstruct.2021.113764>
- Zhao, S. Y., & Xue, P. (2014). New two-dimensional polynomial failure criteria for composite materials. *Advances in Materials Science and Engineering*, 2014(1), 503483.



© 2026 by the authors; licensee Growing Science, Canada. This is an open access article distributed under the terms and conditions of the Creative Commons Attribution (CC-BY) license (<http://creativecommons.org/licenses/by/4.0/>).